Evaluation of the NASA GISS Single Column Model Simulated Clouds Using Combined

Surface and Satellite Observations

Aaron D. Kennedy, Xiquan Dong, and Baike Xi

Department of Atmospheric Sciences, University of North Dakota, Grand Forks, ND

Patrick Minnis

NASA Langley Research Center, Hampton, VA

Anthony D. Del Genio and Audrey B. Wolf

NASA Goddard Institute of Space Studies, New York City, NY

Mandana M. Khaiyer

Science Systems and Applications, Inc., Hampton, VA

Corresponding author address: Mr. Aaron Kennedy, The Department of Atmospheric Sciences, University of North Dakota, 4149 Campus Road, Box 9006, Grand Forks, ND 58202-9006. Email: aaron.kennedy@und.nodak.edu. Phone: 701-777-4478.

1

Abstract

Three years of surface and Geostationary Operational Environmental Satellite (GOES) satellite data at the Department of Energy Atmospheric Radiation Measurement (ARM) Southern Great Plains (SGP) site are used to evaluate the NASA GISS Single Column Model (SCM) simulated clouds from January 1999 to December 2001. The GOES derived total and high cloud fractions for both 0.5^o and 2.5^o grid boxes are in excellent agreement with surface observations, suggesting that ARM point observations can represent large areal observations. Compared to the ARM observations, the SCM simulated most mid-level clouds, overestimated low clouds (8%), and underestimated total and high clouds by 6% and 12%, respectively. To examine the dependence of the modeled high and low clouds on the synoptic pattern and large-scale variables such as relative hunmidity (RH) and pressure vertical velocity (omega), North American Regional Reanalysis (NARR) data are included. The sucessfuly modeled and missed high clouds are primarily associated with a trough and ridge upstream of ARM SGP, respectively. The PDFs of observed high and low occurrence as a function of RH reveal tha thigh clouds have a Gaussian-like distribution with mode RH values of ~50%, whereas low clouds have a gamma-like distribution with the highest cloud probability occurring at RH ~ 80-90%. The PDFs of modeled low clouds are similar to those of observed ones, however, for high clouds the PDFs are shifted to higher RH than observed which results in a negative bias of high clouds because many are observed below the specified stratiform paramterization threshold RH of 60%. Observed clouds are well correlated with RH and omega fields, especially in the upper troposphere. Modeled clouds are primarily correlated with low-level RH and 300-hPa vertical motion. While ARM forcing and NARR RH fields are similar to each other, significant differences exist for omega.

1. Introduction

Clouds are one of the most important elements in the Earth's hydrology and energy cycles, acting particularly through precipitation processes (Del Genio et al. 2005a) and the Earth's radiation budget. Their treatment in weather forecast and climate models is a significant source of error and uncertainty (Gao and Li 2007; Cess et al. 1996; Randall et al. 2006). Although considerable uncertainty still surrounds cloud feedbacks in General Circulation Models (GCMs), one can assume that to reasonably simulate future climate, these models should be able to accurately reproduce the current climatology of all clouds at a given location. Due to the complexities of GCMs, the Single Column Model (SCM) approach was developed to evaluate parameterizations (Randall et al. 1996) and has been implemented by the Atmospheric Radiation Measurement (ARM) program (Ackerman and Stokes 2003) to improve the representation of clouds and radiation in GCMs using long-term surface observations (Klein and Del Genio 2006).

SCM versions of GCMs typically have been used to simulate the atmosphere over limited time periods, driven by field experiment data or enhanced soundings during intensive observing periods (IOP, see JGR special issue, 2005). These exercises have proven difficult to interpret, because model-data discrepancies can be due to inaccurate large-scale advective forcing, inaccurate model physics, or problems with the cloud data, and instantaneous model errors may not be climatically representative or diagnostic of problems with the model's cloud feedback (Del Genio et al., 2005b). Therefore, it is necessary to use a longer time series to have a statisitically meaningful comparison.

Compared to observations from the International Satellite Cloud Climatology Project (ISCCP; Rossow and Schiffer, 1999) and the Clouds and the Earth's Radiant Energy Ssytem (CERES, Wielicki et al. 1998; Minnis et al. 2008,2009), Zhang et al. (2005) found that the

majority of GCMs only simulated 30-40% of observed mid-latitude mid-level top clouds and half of the GCMs underestimated low-level top clouds, however, not at a statistically significant level. Limitations in the passive satellite data prevented a thourough analysis of high clouds.

To ensure that climate models reliably represent clouds, the parameterizations of cloud-radiation-precipitation interactions and the associated heating and other feedbacks in the models should faithfully represent what is found in nature. Therefore, the time-dependent frequency distributions of cloud properties from the model should also be compared to those derived from observations. Ultimately, improved cloud parameterizations can only result from an integrated analysis of all available data sets, including long-term surface and satellite observations, single column models, and reanalyses.

To provide a much-needed source of long-term cloud-radiation data for evaluating model parameterizations, the ARM Program established the Southern Great Plains (SGP) site, centered near Lamont, Oklahoma, in 1993. ARM has also included satellite observations to determine cloud and radiative properties (Minnis et al. 1995, 2001) to complement the surface data, provide large-scale averages, and bound the radiation budget at the top of the atmosphere (TOA),. In addition to the surface and satellite measurements, Xie et al. (2004) developed the continuous forcing product (1999-2001) over the SGP site. This product is often of a quality comparable to that from Intensive Observing Periods (IOP) and has the advantage of being available for driving SCMs over long periods (Del Genio et al. 2005b).

This paper reports on a continuous period of long-term surface and satellite observations, SCM simulations, and their association with large-scale synoptic patterns and large-scale variables provided by the North American Regional Reanalysis (NARR) over the ARM SGP site. Although the evaluation of an individual SCM driven by a forcing dataset at one location

may have limited practical usage, the ARM SGP site is representative of a continental climate in the mid-latitudes. This paper also investigates the seasonal and vertical variations of observed clouds and their relationship to relative humidity and vertical motion which are widely used as independent variables in GCM stratiform and convective cloud paramterizations in climate models. The paper is formatted as follows. Section 2 gives a brief description of the different datasets used in this study. In section 3, satellite and surface observed clouds are compared to the SCM simulations on hourly, monthly, and seasonal timescales. SCM performance is investigated within section 4 with the aid of large-scale parameters obtained from NARR and ARM Forcing. Section 5 discusses and analyzes the seasonal and vertical variations of clouds with relative humidity and vertical motion. Pertinent conclusions are summarized along with plans for future work in the final section.

2. Datasets

Surface, satellite, ARM continuous forcing, and NARR reanalysis data sets have been collected at ARM SGP during the period 1999-2001 for this study. Because the ARM continuous forcing is required to run the GISS SCM and is only available during 1999-2001, model results are compared with both surface and satellite observations for this 3-yr period. Both the surface and satellite data sets are averaged into hourly means to match the SCM hourly temporal resolution although their spatial resolutions are different.

a. Surface Observations

The DOE ARM 35-GHz Millimeter Wavelength Cloud Radar (MMCR) has a minimum detectable reflectivity factor (Z) of -55 dBZ at 1 km and -35 dBZ at 10 km (Moran et al. 1998). The MMCR operates at a wavelength of 8 mm in a vertically pointing mode and provides

continuous profiles of radar reflectivity from hydrometeors moving through the radar field of view (FOV), allowing the identification of clear and cloudy conditions. The beam width is 0.2° which results in a horizontal resolution of ~40m at 12km AGL. Cloud-top height (Z_{top}) is derived from MMCR reflectivity profiles with an uncertainty of 90 m. The lowest cloud-base height (Z_{base}) is derived from a composite of Belfort laser ceilometer, Micropulse Lidar (MPL), and MMCR data (Clothiaux et al. 2000). Inclusion of the lidar allows for the filtering of insects which produce a significant reflectivity during the spring and summer seasons over the ARM SGP. Another source of error in the cloud radar retrievals is attenuation during precipitation events, which leads to underestimated cloud top heights. To mitigate this issue, only precipitation-free times are considered. This is expected to cause a negligible amount of negative bias to cloud fractions derived for all levels; only 1.4% of all 5-minute samples recorded precipitation.

The cloud fraction (CF), derived from the upward-looking narrow FOV radar-lidar pair of measurements, is simply the percentage of returns that are cloudy within a specified sampling time period, i.e., the ratio of the number of hours when clouds were detected to the total number of hours when both radar and lidar/ceilometer instruments were working.

b. Satellite Observations

The satellite cloud products (Minnis et al., 2001) were retrieved using algorithms developed for the NASA Clouds and Radiant Energy System (CERES) project. Cloud properties were retrieved from half-hourly, 4-km 0.65, 3.9, 10.8 (infrared, IR), and 12.0-μm radiances taken by the eighth Geostationary Operational Environmental Satellite (GOES). Cloudy pixels were identified using an adaptation of the method described by Minnis et al. (2008a). The Visible

6

Infrared Solar-Infrared Split-window Technique was applied during daytime (solar zenith angle < 82°) and the Solar-infrared Infrared Split-window Technique (SIST) was used at night (solar zenith angle >82°) to derive cloud properties for those pixels (Minnis et al. 2009). The areal fraction of clouds (instantaneous cloud amount from the satellite FOV) is the ratio of the number of pixels classified as cloudy to the total number of pixels within a specified area (0.5°x0.5° in this study). The primary technique for determining effective cloud height (H_{eff}) is to estimate effective cloud temperature (T_{eff}) based on the 10.8-μm radiance adjusted to account for cloud semitransparency first, and then to define H_{eff} as the lowest altitude having T_{eff} from a vertical temperature profile based on a sounding or a numerical weather prediction (NWP) model analysis. In this case, the algorithm uses atmospheric profiles obtained from the Rapid Update Cycle 2 (RUC-2; see Benjamin et al., 2004) analyses. The profiles are altered at altitudes below the 500-hPa level using a lapse rate anchored to the 24-h running average surface temperature as described by Minnis et al. (2009). This study uses the gridded layer-averaged GOES-8 cloud amounts (Palikonda et al., 2006; data available at http://www-angler.larc.nasa.gov/). According to the retrieved H_{eff}, the GOES-derived clouds can be classified as low (<2 km), middle (2-6 km), and high (>6 km) clouds. Total cloud coverage is simply the sum of the low, middle and high cloud amounts determined from the GOES data.

c. NASA GISS SCM

The model analysis in this paper uses an archived run of the NASA GISS SCM that is identical to the one described in Del Genio et al. (2005b). The model is based on the SI2000 version of the GCM, but with cloud and convection physics updates described in Del Genio et al. (2005a). The SCM has 35 vertical layers and an implied horizontal resolution of 2°×2.5°

corresponding to a grid box of approximately 220 km square at the SGP. The continuous forcing driving this SCM run uses constrained variable analysis with RUC-2 hourly analyses as the background field (Zhang et al. 2001, Xie et al. 2004). These hourly analyses are constrained by ARM surface and GOES-8 satellite observations to balance observed mass, momentum, heat, and moisture budgets within the column. The model is run hourly from the observed advective temperature and moisture tendencies and is reinitialized at the beginning of each day to remove climatic drift (Del Genio et al. 2005a).

The SCM predicts cloud water but uses an RH-based scheme to diagnose large-scale cloud fraction (Sundqvist et al. 1989, Del Genio et al. 1996) which requires a tunable threshold relative humidity parameter, U_{00}. Commonly set around 60%, stratiform clouds are not allowed to occur below this value. Above this threshold, cloud amount (fraction) is assumed to increase with grid box mean RH. U_{00} is held constant globally and vertically, and only varies (relative to saturation over liquid water) when temperatures are colder than -35ºC to account for the difference between saturation vapor pressure over ice rather than water. For this reason and also because the convective scheme separately diagnoses a convective cloud cover, the SCM can occasionally create clouds at values below the prescribed threshold (Del Genio et al. 1996). The convective scheme uses mass flux and is closed by moving enough mass to neutralize cloud-base instability (Del Genio and Yao 1993). This scheme allows for up to two convective cloud tops (such as cumulus and cumulonimbus) and cirrus anvils by detraining \water vapor/condensate from the convective scheme into the gridbox, where the subsequent evolution is handled by the stratiform scheme.

d. North American Regional Reanalysis (NARR)

The NCEP North American Regional Reanalysis (NARR, Mesinger *et al*. 2005) is a long-term (1979-2007) climate data set with 3-hr temporal, 32-km horizontal, and 45-layer vertical resolutions over the North American domain. It contains outputs of all atmospheric variables and fluxes, and it is nicely suited for diagnosis of synoptic and mesoscale conditions over the ARM SGP site. NARR uses the operational NCEP ETA model and its 3D-VAR data assimilation technique on a wide variety of observation platforms. The end result is a dataset that improves in almost all areas over the earlier global reanalysis dataset.

3. Evaluation of the NASA GISS SCM Simulations

a. Methodology

Although the ARM radar-lidar observations provide the most reliable vertical distributions for verifying the GCM simulations, large-scale satellite data are critical for evaluating GCM simulated spatial distributions of clouds because they provide a means to account for the scale differences between the SCM and surface site. Comparisons between the ground- and satellite-based observations must be conducted carefully because of significant spatial and temporal differences between the two different observing platforms. The differences between the satellite and surface observations must be reconciled before those observations can be used to validate the model simulations. For example, under what conditions are the surface point observations representative of the large grid box of satellite observations? Xi et al. (2009) have shown that there is excellent agreement in long-term mean CFs determined from the 10-yr surface and GOES data. The CF is independent of temporal resolution and spatial scales, at least, up to the size of a 2.5° grid box providing there are enough samples. Cloud frequency of

occurrence increases and mean instantaneous cloud amount decreases with increasing averaging time and spatial scale.

The temporal, spatial, and vertical resolutions of surface radar-lidar and GOES observations and SCM simulations are listed in Table 1. To have the same temporal resolution for the three data sets, both the surface and GOES data sets have been averaged into hourly means to match the SCM hourly outputs. Since GOES can provide only three levels (low, middle, and high) of clouds, both surface (90-m resolution) and SCM (~25-hPa resolution) vertical distributions of clouds have been binned into those three levels to make a reasonable comparison. For spatial resolution, the 0.5°×0.5° grid box of GOES observations have been extended into a 2°×2.5° grid box to match the SCM domain. Figure 1 shows an enlarged 2.5° grid box including the percentages of area from each 0.5° grid box.

Satellite observations may include several error sources that can significantly impact the derived instantaneous cloud amount. In particular, observational noise or retrieval errors can lead to positively biased cloud frequencies for the 0.5° grid box because more clouds occur for very small instantaneous cloud amounts (<5%). Figure 2a illustrates the hit rate (fraction of hours during which satellite and radar observations agree) as a function of the instantaneous GOES cloud amount threshold used here to discriminate between cloudy and clear scenes. The impact of noise or retrieval errors is easily seen for low clouds where their hit rate increases to a maximum at ~10% cloud amount and then is asymptotic to a hit rate of 0.8. This in turn impacts the total cloud hit rate. This suggests that for the best agreement between radar and satellite observations, a threshold instantaneous cloud amount must be set to discriminate between cloudy and clear scenes on an hour-to-hour basis. Other than a minimum below 2%, hit rate slowly decreases for high clouds. This indicates that setting a threshold too high would arbitrarily

classify correct retrievals of clouds by the satellite as clear. Except for optically thin cirrus, satellites should detect most high clouds. Figure 2b demonstrates the impact of the prescribed cloud amount thresholds on the GOES-derived CF. Small cloud amount thresholds alter the derived cloud fractions by a negligible amount (less than 1%). To filter out GOES observational noise and/or retrieval errors and to keep more cloud samples within the SCM domain, a threshold of 5% GOES cloud amount was used to discriminate cloudy ($\geq$5%) and clear (<5%) scenes in this study.

To further investigate the 5% threshold, consider Fig. 3 which illustrates the frequencies of GOES-observed (before applying the 5% threshold) and SCM-simulated cloud amounts. The distributions of GOES cloud amount are characterized by being bimodal for high clouds and exponentially decreasing for the low- and mid-level clouds. Note that the cloud amounts within the first bin of all three levels are less than 5% and have been filtered out in this study. Even if some of these scenes are realistic, the radiative impact of such a small cloud fraction is probably minimal on climatic scales. Despite the large peaks in the first bin of Fig. 3, the distributions are consistent with the Zhang et al. (2003) study which explored GOES cloud amount distributions over a 9.5°×13.5° area centered on the ARM SGP during a summer month. Modeled three-level cloud fractions peak at large cloud amounts (>85%) while others are nearly equally distributed from 5% to 85%. This is most likely caused internally within the SCM cloud parameterization scheme when volumetric cloud fraction is converted into the horizontal scale.

b. Cloud Fraction and Frequency

For the GOES results, the cloudy frequency of occurrence FREQ is taken to be 0 for instantaneous cloud amount AMT < 0.05 and 1 when AMT $\geq$ 0.05. The monthly averaged AMT

is the average of all hourly AMTs (>0.05) and represents the averaged cloud amount when clouds are present. The average FREQ (probability of cloud occurrence) is the ratio of the number of times AMT>0.05 to the total number of satellite observations during that month. Finally, the monthly mean CF is defined as the product of the monthly averaged instantaneous AMT and FREQ. This is equivalent to the CF derived by the radar-lidar observations if clouds occur uniformly over the domain. This assumption is valid at the ARM SGP on scales of months, seasons, and years (Xi et al. 2009).

1) DIURNAL VARIATION OF CLOUD FRACTION

The diurnal variations of hourly mean total and three-level CFs are illustrated in Fig. 4. The diurnal cycles are plotted in UTC (SGP local time=UTC - 6 hours) because the SCM was reinitiated at 00 UTC every day with no spin-up period. For surface observations, diurnal variations primarily occur for low clouds, which are typically subject to mesoscale or microscale forcing with the rise/set of the sun. There are more low-level clouds in the morning than during the afternoon. Very little variability occurs for clouds above 6 km which are more often tied to large-scale forcing independent of the diurnal cycle. Other than anvil cirrus clouds due to afternoon/evening thunderstorms, high-level clouds are often associated with the large-scale forcing, such as ascent with baroclinic waves.

For GOES-derived CFs, there is no strong diurnal variation for total clouds, but there is a significant drop for high clouds and an increase in both low and middle clouds around sunrise (~12-13 UTC in Fig. 4). This is primarily due the effect of multilayered clouds on the different retrieval algorithms used for day and night. The increased low and midlevel CF during daytime is mainly due to the fact that high, thin cirrus over low clouds only slightly diminishes the IR brightness temperature T_{IR}, but the visible channel indicates that the cloud is optically thick. The

12

net result is that the VISST assumes that the T_{eff} is essentially the same as T_{IR}. Thus, the VISST retrievals for thin-over-thick multi-layered cloud systems yield a low or midlevel cloud depending on the altitude of the lower cloud and the optical thickness of the upper-level cloud. If the upper-level cloud has an optical depth greater than about 3 or so, the cloud is interpreted as a high cloud and the lower cloud is undetected. Even in single-layered cirrus cases, the cloud height is underestimated (Smith et al., 2008) because the cirrus optical depth is overestimated (Min et al., 2004).

At night, however, the SIST is relatively insensitive to the presence of a low-level cloud underneath a thin high cloud because the surface and low-cloud temperatures typically differ by only a few degrees. Thus, the upper-level cloud is detected as being semi-transparent and T_{eff} differs significantly from T_{IR} and a relatively accurate high-cloud altitude results fro both single (Smith et al., 2008) and multi-layered clouds. The low clouds underneath the cirrus are not detected. If the upper-level cloud is optically thick, the underlying low and midlevel clouds will not be detected Therefore, it is possible for GOES to miss some low-level clouds underneath optically thin cirrus clouds during the nighttime and/or low clouds with similar brightness temperatures as the ground. These algorithmic effects result in the high cloud CF decreasing from nighttime to daytime, which corresponds to an apparent increase for low and mid-level clouds. The low and midlevel cloud amounts are always less than the values from the radar because of the screening effect of the high clouds.

The SCM simulated clouds monotonically increase from 00 UTC to local noon (~18 UTC) for total and all three-level clouds as shown in Fig. 4. The day (12 − 24 UTC) minus night (0 − 12 UTC) cloud fractions differences vary by 28-37% depending on the level. Although other issues cannot be completely ruled out, the culprit for this steady increase in CF is mainly

due to the 00 UTC daily initialization for the model. As might be expected, this model spin-up time (~12 hours as shown in Fig. 4) would introduce a negative bias to all cloud fraction calculations. Therefore, all CFs derived from surface, GOES, and SCM datas are based only upon the 12 – 24 UTC time period.

2) SEASONAL VARIATION OF CLOUD FRACTION AND FREQUENCY

The monthly variations of total, high, middle and low cloud fractions and frequencies derived from surface radar-lidar, 0.5^o and 2.5^o grid boxes of GOES observations, and SCM simulations at the SGP site during the 3-yr period are illustrated in Fig. 5. Their corresponding annual means are summarized in Table 2. Both the surface and GOES-derived total CFs agree very well in general trend and magnitude with almost identical annual means. They both peak during the January-March period, have a second peak in June, followed by a significant drop into July, finally increasing from summer to winter. The monthly variations of the three-level CFs basically follow the total CF trend with minor variations. Although the GOES-derived high CF is 0.1 – 0.2 less than that from the surface, the high-cloud frequency agrees well with the surface observations suggesting that at least part of the high cloud cover is correctly identified whenever high clouds occur during the daytime. Middle and low CFs are less than the surface observations throughout the year except for the July-August period. This is understandable because some of the middle and low clouds are masked by upper level clouds. The fact that some of the low and mid-level clouds are actually misidentified high clouds, as discussed above, is reinforced by their greater frequencies of occurrence as seen by the satellite. Although these comparisons are not long enough to represent a climatology of clouds over the SGP site, it is concluded that they are

typical because the seasonal variations of clouds in this study are very similar to other studies that used longer time series (Dong et al. 2006, Xi et al. 2009).

Despite being consistently less than observations, the monthly variations of SCM-simulated total and three level clouds undergo seasonal changes that are somewhat similar to those observed from the surface and satellite with one exception. The SCM midlevel CF maximum is several months out of phase with the others, however, still corresponds with a local maximum in the observations. As seen in both Figs. 4 and 5, the SCM simulates significantly fewer clouds overall (~10%) than detected by the observations regardless of the overlap assumption used. Investigation of individual layers reveals that the SCM simulated most middle and low cloud cover compared to the surface and GOES observations. The SCM underestimated high clouds fractions relative to the surface data, but yields remarkably good agreement for high clouds with no the no overlap assumption compared to satellite observation.

The monthly variations of cloud frequencies are nearly the same as their CF counterparts except with relatively large values. As expected, the observed cloud frequencies are greater for the large grid box (2.5°) than for the small grid box (0.5°) and ARM surface observations, i.e., the cloud frequencies increase with larger spatial scales. For high clouds, the 0.5° grid box of GOES and radar observed cloud frequencies are nearly equivalent, which suggests that on the order of an hour, radar observations are a good approximation for a 0.5° grid box of satellite observations. The SCM simulated cloud frequencies are lower than observed ones except for low clouds. For high clouds, the SCM frequency is nearly the same as the corresponding CF (0.16 vs. 0.15), which indicates that the model simulated either clear skies or scenes with large cloud amounts. This argument is also supported by Fig. 3a.

Table 2 summarizes the 3-yr averaged cloud fractions and frequencies for total and three-level clouds. The percentages of surface and GOES observations and SCM simulations used are 84%, 93%, and 100% of all possible data during the 3-yr period, respectively. As listed in Table 2, the GOES-derived total CFs from both 0.5° and 2.5° grid boxes are in excellent agreement with surface observations, while for individual cloud layers the limitation of GOES satellite observations is apparent, all three of the layer CFs are less than the surface results. This discrepancy can be explained as follows: 1) the difficulty of cloud base detection for passive sensing satellites, 2) missed or underestimated H_{eff} for optically thin cirrus clouds, 3) missed low-level clouds when optically thick cloud layers are present above, and 4) the limitation of nighttime retrievals without visible channels. Despite the difficulties in detecting these lower clouds, the good agreement of the total and high cloud categories for satellite and radar observations provides strong evidence that the long-term observations of CF at the ARM SGP site are representative of a large grid box of satellite observations. It is expected that the 0.5° GOES-derived CFs should be more representative of the surface-retrieved CFs than the larger-scale averages. Thus, since the total CF for the smaller box is 0.02 greater than that for the 2.5° box, it can be assumed that differences in cloud cover less than ~0.03 between the large-scale SCM and the surface site are insignificant.

3) VERTICAL AND MONTHLY DISTRIBUTION OF CLOUD FRACTIONS

To evaluate the vertical and monthly distribution of SCM simulated clouds, ARM MMCR data were binned into the same vertical resolution of the model (~25 hPa). Figure 6 shows the monthly mean time-height series of cloud fractions derived from ARM MMCR observations and simulated by the GISS SCM over the ARM SGP, as well as their differences during the 3-yr period. The observed cloud fraction has a bimodal distribution with peaks in the

high levels at approximately 300 hPa and another near the top of the boundary layer at ~850 hPa. The largest cloud fractions occur during the late winter and early spring seasons when baroclinic wave activity is common over the ARM SGP site. High cloud fraction also varies somewhat by height with the fall and rise of the tropopause by season due to the thermal thickness of the atmosphere.

The simulated CFs in Fig. 6b differ substantially from the observed values. Aside from the aforementioned overall lack of high clouds and excess of low clouds, several specific seasonal errors exist: (1) the observed late winter peak in 300-hPa cloud is missing in the SCM, (2) The overproduction of boundary layer clouds is most prominent during the late winter and early spring with values of 5-10% over the observed CF. Given that the model uses a stratiform scheme that is based on grid box mean RH, this is consistent with time periods of aforementioned wave activity and/or Low Level Jets (LLJ). In fact, there are some distinct similarities with the climatology of the LLJ over the ARM SGP in the Whiteman et al. 1997 study that found that low-level clouds peaked during the months of June and October.

The time-height series of modeled cloud fractions in Fig. 6 raise the following question: are the consistent differences between the observed and SCM-simulated clouds caused by the model cloud parameterizations, by clouds that are forced on a scale irresolvable by the model and its forcing, or by errors in the ARM continuous forcing? The cloud parameterizations within the NASA GISS SCM use large-scale variables, such as RH and cumulus mass flux, to predict clouds. Changes in the model-observation clouds with season and height suggest that either the relationships of cloud cover with these parameters vary seasonally or advective forcing is variable by season. High clouds, for example, are underestimated regardless of season, and very few are produced during the summer. This bias could be explained by a variety of mechanisms.

Climatologically, Oklahoma is dominated by large-scale ridging during the summer. With plentiful subsidence and the lack of baroclinic waves to transport moisture to the upper atmosphere, its RH is lower than during other seasons. Considering that the model uses both RH and cumulus mass flux to forecast clouds, it is not difficult to fathom less cloud cover being simulated during the summer months. Another plausible explanation may be that the model cannot simulate an adequate amount of sub-grid scale convection thereby generating fewer cirrus anvils from convective clouds during the summer. The consistent negative bias of high clouds, however, suggests an issue exists regardless of cloud forcing. To partially answer the questions and test the various hypotheses, the association of model clouds with NARR-derived synoptic pattern and ARM continuous forcing is explored in the following sections.

4. Association of the observed and modeled clouds with large-scale synoptic pattern

To match the temporal resolution of the NARR dataset, the radar observations and SCM simulations were reduced to 3-hourly time steps for this portion of the study. For simplicity, each time step is classified as either clear or cloudy, and cloud fraction is not considered. To best represent the upper level synoptic pattern, the 500-hPa geopotential height and vertical motion (omega < 0 for upward and > 0 for downward) and 300-hPa RH were selected to study high clouds. For low clouds, mean sea level pressure (MSLP), 500-hPa omega, and 925-hPa RH were considered. These three parameters were then averaged for the following conditions: 1) periods when clouds were both observed and simulated (hit) and 2) clouds were observed but not simulated (miss). For brevity, these are referred to as hits and misses, although they are not quite the same as the more commonly used terminology that includes correct and incorrect simulations of null forecasts (no cloud).

a. High clouds

Figure 7 illustrates the 500-hPa geopotential height and vertical velocity and 300-hPa relative humidity anomalies (relative to the 3-yr period) for both the modeled and missed high clouds over the SGP during the 3-yr period. The 500-hPa geopotential height field for model hits (Fig. 7a) is characterized by a dipole pattern with negative (positive) anomalies from climatology west (east) of the SGP. This is indicative of a trough upstream of the site for model hits. The maximum negative geopotential height anomalies are approximately 20 m below the climatological geopotential height of observed high clouds and are within the 99% significance level. Model hits are also associated with strong upward motion in the omega field (Fig. 7b) and positive relative humidity anomalies (Fig. 7c). The entire model domain is easily within the 99% significance level with a peak vertical motion anomaly of -0.08 Pa s^{-1} and an RH anomaly of 5%.

Model misses are characterized by a reversal in the NARR fields, which nearly mirror the synoptic pattern for model hits. Geopotential height anomalies are consistent (Fig. 7d) with a ridge to the west of ARM SGP. Although this pattern is statistically significant, the amplitude is less than that of the trough (15 m). Likewise, model misses are associated with sinking motion and drier conditions. These fields, while significant at the 99% level, have magnitudes less than those associated with the trough with 0.06 Pa s^{-1} for omega and -4% for RH.

These results are consistent with the hypothesis that the model is primarily producing high clouds during synoptically evident events. High clouds are typically formed when a trough lies west of ARM SGP. From quasigeostrophic theory, one would expect rising motion to occur east of the trough axis and with this rising motion, increased moisture transport to the upper troposphere. Model misses, however, occur when clouds are associated with large-scale ridging.

Associated with this ridging is sinking motion and negative RH anomalies. At least some of the missed high clouds can be explained through this analysis. During the periods when there are few baroclinic waves, high CFs will be smaller. This normally occurs over the SGP region during the summer months when the polar jet is shifted farther north. Given that high clouds still occur frequently during the summer, however, this suggests that these occur due to sub-grid scale forcing, such as local thunderstorms. This argument is reinforced by the values in Table 3 which presents the percentage of cloud fraction that occurs during the periods of 500-hPa sinking motion. Over one third of the high cloud cover is associated with neutral or sinking air motion at the 500-hPa level. During the summer, this number increases to nearly one half. The modeled cloud fraction averages are only ~20-25 % (compared to the observed 32-47% CF) which suggests that stratiform scheme is suspect in generating enough high cloud cover. Is it possible for this parameterization within the SCM to accurately simulate a realistic amount of high cloud?

b. Low clouds

The relationship of low clouds with NARR fields is given in Fig. 8. Model hits are characterized by lower MSLP (Fig. 8a), weak rising motion (Fig. 8b), and positive RH anomalies (Fig. 8c). Although the patterns are consistent with the results for high clouds and significant at the 99% level, the magnitude of these fields is much lower: 1 hPa, -0.01 Pa s^{-1}, and 4%, respectively. The weak relationship to 500-hPa vertical motion can be explained by low clouds being controlled by PBL processes. The weak relationship of low clouds with RH is somewhat surprising, however.

Anomalies for model misses are opposite of those for hits, but are much greater in magnitude. Values over the ARM SGP are 3 hPa for MSLP, 0.08 Pa s^{-1} for omega, and -14% for RH. While their patterns are asymmetric compared to those of high clouds, the most striking

difference is the large difference in magnitude. To help explain this result and also answer the questions raised for high clouds, it is necessary to examine the seasonal and vertical variations of clouds related to the RH and omega fields from both ARM forcing and the NARR datasets.

5. Relationships between clouds and large scale parameters

Considering most missed clouds occur during quiescent conditions with neutral or sinking vertical motion, scrutiny will focus on the stratiform cloud parameterization. In particular, what is the association of observed clouds with RH under such conditions? How well does the current stratiform threshold of U_{00}=60% RH in this model run represent the SGP conditions? Because the SCM simulations are dependent on the ARM continuous forcing dataset driving this run, it is also necessary to compare this dataset with NARR.

a. Relationship of RH to high and low clouds

The probability of a given ARM-forced RH occurring for observed and modeled high cloud scenes are illustrated in Fig. 9a. The observed high cloud distribution is near-Gaussian with a peak near 50% whereas the model's peak is at ~70% RH for total and stratiform cloud fractions. This is a function of the cloud parameterizations used in the model and suggests that the model could produce more clouds if U_{00} was simply lowered. While not shown, the probability distribution function (PDF) of RH for all clear and cloudy scenes shows that the SCM produces higher RH, and fewer low RH values than indicated by the continuous forcing at the SGP, suggesting a shortcoming in the forcing advection at high altitudes. Together, the tendency for high RH values and the parameterization specification that restricts stratiform cloud

to high RH cause the probability of high cloud to increase nearly exponentially with RH, a feature not seen in the data (Fig. 9b).

For low clouds, several differences exist. The probability of RH for cloudy scenes (Fig. 9d) has a gamma-like distribution with a peak at ~85% RH and a sharp drop off towards RH = 100%. The model histogram has a similar shape and peak value but is more strongly peaked. The PDF for RH occurrence (not shown) also has too many high RH values, as for high clouds, but is otherwise similar in shape to the observations. Unlike high clouds, the probability of observed low clouds occurring at high RH is much lower with only a 60% probability at RH values of 95-100% (Fig. 9d). In the SCM, the cloud probability increases sharply with RH > 60% consistent with the specified U00. Because the majority of low clouds occur at high RH, there is little difference for periods with both observed and simulated clouds. Misses on the other hand occur frequently when low clouds occur at RH values well below the threshold.

b. Seasonal and Vertical Relationship of Clouds with the RH and Omega fields

Figure 10 shows the monthly mean vertical distributions of the RH field under all-sky (left), cloudy (middle) conditions, and their differences (right) for both ARM continuous forcing and NARR SCM grid box mean. Mean RH plots for both ARM (Fig. 10a) and NARR (Fig. 10b) share a striking resemblance in the upper troposphere with the observed cloud fractions in Fig. 6a. Local maxima occur in both figures during the months of January, March, and June. While the relationship for low clouds is less clear, some association between high boundary layer humidity and cloud fraction near the top of the PBL appears to exist. Modeled low cloud fraction peaks during months with high RH values in the lower levels. The ARM and NARR datasets are in relatively good agreement (Fig. 10c) with values within several percent in the free

atmosphere. The largest differences occur within the PBL and above the tropopause where the ARM forcing has a significant positive bias (~10-15%).

The mean RH during cloudy conditions is characterized by a decrease with height and lower values during the summer months (Fig. 10 d-e). Several month-to-month RH differences between ARM and NARR exist during January and March which also correspond well with those RH differences during all-sky conditions. The largest RH differences (~10%) between ARM and NARR occur once again in the PBL (Fig. 10f).   The remainder of the troposphere is characterized by differences on the order of 2% in magnitude except during the winter and late spring where the ARM RH is 6-8% higher than NARR values.

The RH anomalies between cloudy and all-sky conditions are shown in Fig. 10g-i. Larger anomalies indicate a stronger dependence of clouds on RH values and suggest that more clouds can be resolved at the resolution of the forcing (non sub-grid scale). There are strong seasonal variations in the ARM RH differences (Fig. 10g) from the surface up to 400 hPa, ranging from 0-5% between 850-700 hPa during summer months to 30-35% between 850-600 hPa in December. The NARR RH differences mimic the seasonal variations of ARM values with a decreased magnitude. While the ARM and NARR data are similar in shape and location of minima and maxima, ARM has a consistent positive bias of 2% over most of the troposphere and 6% during the winter months. The maximum RH difference (~10% in Fig. 10i) occurs in the upper troposphere during October, which appears to be caused by the difference in mean RH between ARM and NARR for that month.

As was done for RH, the seasonal and vertical relationship of clouds to the omega field was investigated (Fig. 11). Contrary to RH, the ARM AND NARR omega fields differ quite markedly as shown in Fig. 11a-b. For ARM, the omega field is characterized by having strong

upward motion (<-0.05 Pa s^{-1}) during April-June in the middle troposphere. Other peaks during March and September, and October, however, were weaker in amplitude. While the observed cloud fraction has a strong resemblance to the mean RH field, the modeled cloud fraction is somewhat similar to the ARM mean omega field. Most simulated clouds are associated with the strong upward motion during May-June from 700-300 hPa, which is expected given that it has already been determined the model principally produces clouds during periods of upwelling. The NARR data have smaller amplitudes for rising motion. While month-to-month variations are in good agreement with ARM, NARR has subsidence during the summer months with peak values around 0.03 Pa s^{-1}. As a result, the ARM omega field has a positive bias during the fall and winter seasons and stronger negative bias during the spring and summer.

The ARM mean omega field during cloudy conditions is negative throughout the entire troposphere, with the peaks occurring between 550-330 hPa during April-June (Fig. 11d). The absolute values gradually increase throughout the winter and spring and peak at -0.20 Pa s^{-1} during June- July before dropping off substantially in August. Although the same pattern exists for the NARR data in Fig. 11e, its values are much weaker, similar to the omega comparison for all-sky conditions in Figs. 11 a-b and the RH comparisons. Additionally, values for the NARR omega field peak during February and March instead of the late spring/early summer and from 800-600 hPa instead of 550-350 hPa. The largest omega difference for cloudy conditions ($\sim$ -0.13 Pa s^{-1}, Fig. 11f) occurs during the summer when there are insignificant differences in RH (Fig. 10f). This appears to be related to the one major discrepancy between the two datasets: significant sinking motion throughout the column for NARR during July and August. Because the omega values for cloudy conditions are significantly larger than those for all-sky condition (note the difference in scales in Fig. 11 a-b and d-e), anomalies between the two conditions

within Fig. 11g-i are similar. The key features of the cloud relationship with the omega field over the SGP appear to be the month-to-month variability and also the significant differences between the ARM forcing and NARR datasets. Having already stated how important vertical motion is for cloud production in this run of the NASA GISS SCM, one must question what would occur if the model was driven by forcing developed from the NARR dataset.

c. Correlations of cloud fraction with RH and Omega

To quantitatively investigate how clouds are associated with RH and omega fields, linear Pearson correlation coefficients were calculated between cloud fractions and variables at 925, 500, and 300 hPa for the 36 monthly means. Coefficients were calculated for both ARM and NARR data with the observed cloud fractions and for ARM continuous forcing with the modeled cloud fractions (stratiform+convective).

Correlation coefficients between cloud fraction and RH are listed in Table 4a. For each layer of cloud fraction, the largest values are bolded. The correlations between the observed cloud fractions (three levels and total) and ARM forcing range from moderate to high (0.51-0.85) and generally increase with cloud altitude. The correlations with NARR RH basically follow the patterns of ARM forcing, and are consistently higher than those with ARM forcing, although the differences are negligible for high clouds. The strongest correlations (0.84-0.89) that occur for observed total and high clouds with 300 hPa RH indicate that clouds do correlate well with upper level RH values.   However, the RH-based SCM simulated clouds have only moderate correlations (0.57-0.64) with RH values at 300 hPa, which suggests improvement can be made. Conversely, the modeled low and total clouds have much higher correlations (0.84-0.9) with 925-hPa RH values than those (0.52-0.65) observed clouds. This suggests that many of the high

clouds being simulated are due to deep convection, although further study is needed to confirm this.

Table 4b contains the correlations between cloud fractions and omega values. Because cloud fraction is inversely related to omega values, the strongest correlations approach values of -1. In general, the correlations between observed and modeled clouds and omega values increase from 925 to 300 hPa. The observed clouds (three levels and total clouds) have almost no correlation with both ARM forcing and NARR data at 925 hPa level, however, all correlations increase with cloud altitude and the correlations with NARR are nearly doubled over those with ARM forcing at 500 and 300 hPa levels. The correlations between modeled clouds and ARM forcing are relatively high at 500 and 300 hPa levels, and range from -0.6 to -0.75 with the highest values for high clouds. Notice that the correlations between modeled high clouds and ARM forcing, and between observed high clouds and NARR data are very close (much higher than those between observed high clouds and ARM forcing). This is in part because too few clouds are produced by the stratiform scheme. The close correlation and large difference begs the question: which dataset is more accurate and can the model produce a more accurate simulation if the NARR dataset is used as forcing? These questions are certainly deserved in a further study.

d. Discussion

The results from this section highlight the seasonal and vertical variation of cloud related to RH. In the lower troposphere, a RH threshold of U_{00}=60% captures the majority of low clouds and leads towards an overproduction (positive bias) of low cloud cover due to the amount of clear scenes that occur at RH > 60%. For high clouds, many clouds are observed well below

U_{00}. If the model can only produce high clouds during the periods of upwelling motion or higher humidity in the upper troposphere, it is easily understood why the SCM has a negative bias for high clouds. The best balance occurs in the mid levels where the modeled cloud fraction is similar to radar and satellite observations.

As discussed above, the positive and negative bias for modeled clouds can be resolved by varying the threshold RH value with height, that is increasing it near the surface and lowering it in the upper troposphere. Although a stepped RH threshold has been used in the NCAR CAM3 and cloud-resolving models (Xu and Kruger 1991), it is ill-advised to change the NASA GISS parameterizations at the present time based on this study over one location. Although development of a diagnostic relationship between clouds and large-scale variables such as RH and omega is not too difficult, this is counterintuitive to the prognostic nature of the NASA GISS SCM and disregards advances in physically representing cloud cover. While such a relationship could be implanted under the notion that sub-grid scale variability of clouds varies with height, such an analysis would also "tune" the model to one forcing dataset at one location and it is unknown whether this would hold globally for other climate regimes or even different resolutions.

6. Summary and Conclusions

The NASA GISS SCM simulated clouds over the ARM SGP have been compared with combined radar-lidar and satellite observations during the period 1999-2001. To qualitatively and quantitatively investigate how well the observed and modeled clouds were associated with large-scale synoptic patterns and large-scale variables, the observed and modeled clouds with

ARM forcing and NARR data were explored. Through an integrative analysis of observations, simulations, and forcing/reanalysis datasets, the following conclusions are reached:

1) The GOES-derived total and high CFs from both 0.5° and 2.5° grid boxes are in excellent agreement with surface observations, which proves the ARM point observations can represent large areal observations on yearly and even monthly timescales at a relatively low level (~0.03) of uncertainty. For the middle and low cloud layers, the GOES-derived CFs are less than surface observations because of cloud overlap issues and the limitations of detecting clouds using passive satellite observations. Compared with the surface-GOES observation comparisons, the the SCM simulates most mid-level clouds, overestimates low clouds (8%), and underestimates total and high clouds by 6% and 12%, respectively. The most notable difference between observations and simulations is the lack of modeled high clouds regardless of season. There is no strong diurnal variation for both surface and GOES-derived total clouds. A significant drop in high clouds and a bump in both low and middle clouds around the sunrise (~12-13 UTC) for GOES observations are mainly caused by the usage of two different detection algorithms for day and night.

2) Investigation of NARR data for modeled high clouds reveals that the model hit/missed clouds occur during a trough/ridge upstream of ARM SGP. These synoptic patterns are associated with rising/sinking motion and positive/negative RH anomalies. Modeled clouds are associated with the rising motion that occurred over the east of the trough axis and increased moisture transport to the upper troposphere. The model misses, however, are associated with large-scale ridging, sinking motion and negative RH anomalies. At least part of the missed high clouds can be

explained through this analysis. Fewer high clouds can be produced during the periods when baroclinic wave activity is often absent, a condition that normally occurs over the SGP region during summer months when the polar jet is shifted farther north.

3) The probability distributions of RH occurrence differ for observed high and low cloud scenes. High clouds have a Gaussian-like distribution with a peak at~50% RH, whereas low clouds have a gamma-like distribution with the highest cloud probability occurring at a RH between 80-90%. While the distributions of observed and modeled low clouds are mostly similar, high cloud distributions peak at greater RH values than the observations. Combined with the tendency for the continuous forcing to under predict RH, this results in a simulated cloud negative bias because most observed clouds occur at values below the specified threshold RH of 60%. The cloud probability function shows that simply lowering the threshold at upper levels in the atmosphere can help produce reasonable results and might be justified under the notion that sub-grid scale variability of clouds changes with height. Such a task requires further study and must account for the differences in humidity among models.

4) Time-height plots of RH and omega and related correlation coefficients show that observed clouds are well correlated with RH and omega, especially in the upper troposphere. Modeled cloud fraction is correlated primarily with low-level RH and 300-hPa vertical motion, which suggests that the modeled high clouds are mostly due to the convective scheme. The ARM forcing and NARR RH fields are similar to each other, however, significant differences exist for vertical motion. The higher correlations between clouds and NARR data beg the question:

which dataset (ARM forcing and NARR) is more accurate and can the model simulations be improved if the NARR dataset is used as input? These questions warrant additional study.

The results presented in this study only represent clouds over a single continental area during the 3-yr period. While these findings suggest some possible directions for improvement, similar analyses and tests need to be performed in other climate regimes, such as polar, tropical, and subtropical ocean regions, to see whether the insights achieved are general or location-specific. A variety of other questions remain unresolved. A large percentage of clouds over the ARM SGP are forced on cloud and mesoscales unresolved by the continuous forcing. In particular, convection poses a significant challenge to GCM modelers. How feasible is it for any SCM to diagnose such clouds in the absence of knowledge about the forcing on smaller scales? It may be possible to gather additional statistics on these clouds by incorporating precipitation radars over the SGP site to give a complete picture about convective clouds, including their cores and stratiform regions. Other questions related to the cloud microphysical and optical properties and their impact on the surface and TOA radiation budget are also important. Until these questions are explored in detail, it is impossible to understand the true validity of the NASA GISS GCM/SCM and its cloud parameterizations.

5. Acknowledgements

References

Ackerman, T.P., and G.M. Stokes, 2003: The Atmospheric Radiation Measurement Program, *Phys. Today*, **56**, 38-44.

Bauer, M., and A.D. Del Genio, 2006: Composite analysis of winter cyclones in a GCM: Influence on climatological humidity. *J. Climate*, **19**, 1652–1672.

Cess, R. D., et al., 1996: Cloud feedback in atmospheric general circulation models: An update. *J. Geophys. Res.*, **101**(D8), 12,791–12,794.

Benjamin, S. G., et al., 2004: An hourly assimilation/forecast cycle: The RUC. *Mon. Weather Rev.*, *132*, 495– 518.

Del Genio, A.D., and M.-S. Yao, 1993: Efficient cumulus parameterization for long-term climate studies: The GISS scheme. The representation of cumulus convection in numerical models, *Meteor. Monogr., No. 46*, Amer. Meteor. Soc., 181-184.

Del Genio, A.D., M.-S. Yao, W. Kovari, and K.K.W. Lo, 1996: A prognostic cloud water parameterization for global climate models. *J. Climate*, **9**, 270–304.

Del Genio, A.D., W. Kovari, M.-S. Yao, and J. Jonas, 2005: Cumulus microphysics and climate sensitivity. *J. Climate*, **18**, 2376–2387.

Del Genio, A.D., A.B. Wolf, and M.-S. Yao, 2005: Evaluation of regional cloud feedbacks using single-column models. *J. Geophys. Res.*, **110**, D15S13, doi:10.1029/2004JD005011.

Dong, X., B. Xi, and P. Minnis, 2006: A climatology of midlatitude continental clouds from the

   ARM SGP Central Facility. Part II: Cloud fraction and surface radiative forcing. *J. Climate*,

   19, 1765-1783.

Hogan, R. J., C. Jakob, and A. J. Illingworth, 2001: Comparison of ECMWF winter-season

   cloud fraction with radar-derived values. *J. Applied Metr.*, **40**, 513-525

Kollias, P., E.E. Clothiaux, M.A. Miller, B.A. Albrecht, G.L. Stephens, and T.P. Ackerman,

   2007: Millimeter-wavelength radars: New frontier in atmospheric cloud and precipitation

   research. *Bull. Amer. Meteor. Soc.*, **88**, 1608–1624.

Mace, G.G., E.E. Clothiaux, and T.P. Ackerman, 2001: The composite characteristics of cirrus

   clouds: Bulk properties revealed by one year of continuous cloud radar data. *J. Climate*,

   14, 2185–2203.

Mesinger, F., and coauthors, 2006: North American Regional Reanalysis. *Bull. Amer. Meteor.

   Soc.*, **87**, 343–360.

Min, Q, P. Minnis, and M. M. Khaiyer, 2004: Comparison of cirrus optical depths from GOES-8

   and surface measurements. *J. Geophys. Res.*, **109**, D20119, 10.1029/2003JD004390.

Minnis, P., and coauthors, 2001: A near-real time method for deriving cloud and radiation

   Properties from satellites for weather and climate studies. *Proc. AMS 11ᵗʰ Conf. Satellite

   Metr. and Oceano.*, Madison, WI, Oct. 15-18, 477-480.

Minnis, P., Y. Yi, J. Huang, and K. Ayers, 2005: Relationships between radiosonde and RUC-2

   meteorological conditions and cloud occurrence determined from ARM data. *J. Geophys.

   Res*. **110**, D23204, doi:10.1029/2005JD006005

Minnis, P., and co-authors, 2009: Cloud property retrievals for CERES using TRMM VIRS and

   Terra and Aqua MODIS data. *IEEE Trans. Geosci. Remote Sens.*, submitted.

Minnis, P., W. L. Smith, Jr., D. P. Garber, J. K. Ayers, and D. R. Doelling, 1995: Cloud

   properties derived from GOES-7 for the Spring 1994 ARM Intensive Observing Period using

   Version 1.0.0 of the ARM satellite data analysis program. *NASA RP 1366*, 59 pp.

Minnis, P., and co-authors, 2008: Cloud detection in non-polar regions for CERES using TRMM

   VIRS and Terra and Aqua MODIS data. *IEEE Trans. Geosci. Remote Sens.*, **46**, 3857-3884.

Moran, K.P., B.E. Martner, M.J. Post, R.A. Kropfli, D.C. Welsh, and K.B. Widener, 1998: An

   Unattended Cloud-Profiling radar for use in climate research. *Bull. Amer. Meteor. Soc.*, **79**,

   443–455.

Palikonda, R., and Co-authors, 2006: NASA-Langley web-based operational real-time cloud

   retrieval products from geostationary satellites. *Proc. SPIE Asia-Pac. 5ᵗʰ Intl. Symp., Conf.*

   Rem. Sens. Atmos. & Clouds, **6408**, CD-ROM, 6408-72, 9 pp.

Randall, D.A., K.m. Xu, R.J. Somerville, and S. Iacobellis, 1996: Single-column models and

   cloud ensemble models as links between observations and climate models. *J. Climate*, **9**,

   1683–1697.

Rossow, W. B. and R. A. Schiffer 1999: Advances in understanding clouds from ISCCP. *Bull.*

   Amer. Meteor. Soc., **80**, 2261-2287.

Schmidt, G.A., and coauthors, 2006: Present-day atmospheric simulations using GISS

   Model E: Comparison to in situ, satellite, and reanalysis data. *J. Climate*, **19**, 153–192.

Smith, W. L., P. Minnis, H. Finney, R. Palikonda, and M. M. Khaiyer, 2008: An evaluation of

   operational GOES-derived single-layer cloud top heights with ARSCL over the ARM

   Southern Great Plains site. *Geophys. Res. Lett.*, **35**, L13820, doi:10.1029/2008GL034275.

Sundqvist, H., E. Berge, and J.E. Kristjánsson, 1989: Condensation and cloud parameterization

   studies with a mesoscale numerical weather prediction model. *Mon. Wea. Rev.*, **117**, 1641–

1657.

Xie, S., R. T. Cederwall, and M. Zhang, 2004: Developing long term single-column

   model/cloud system- resolving model forcing data using numerical weather prediction

   products constrained by surface and top of the atmosphere observations, *J. Geophys. Res.*,

   109, D01104, doi:10.1029/2003JD004045

Xu, K.M., and S.K. Krueger, 1991: Evaluation of cloudiness parameterizations using a

   cumulus ensemble model. *Mon. Wea. Rev.*, **119**, 342–367.

Wielicki, B.A., et al., 1998: Clouds and the Earth's Radiant Energy System (CERES): An Earth

Observing System Experiment, *Bull. Am. Meteorol. Soc.*, **77**, 853-868

Wilks, D. S., 1995: Statistical methods in the atmospheric sciences. *Academic Press*, 467.

Zhang, M.H., J.L. Lin, R.T. Cederwall, J.J. Yio, and S.C. Xie, 2001: Objective analysis of ARM

    IOP data: Method and sensitivity. *Mon. Wea. Rev.*, **129**, 295–311.

Zhang, M.J., and coauthors, 2005: Comparing clouds and their seasonal variations in 10

   atmospheric general circulation models with satellite measurements. *J. Geophys. Res*. **110**,

   D15S02, doi:10.1029/2004JD005021
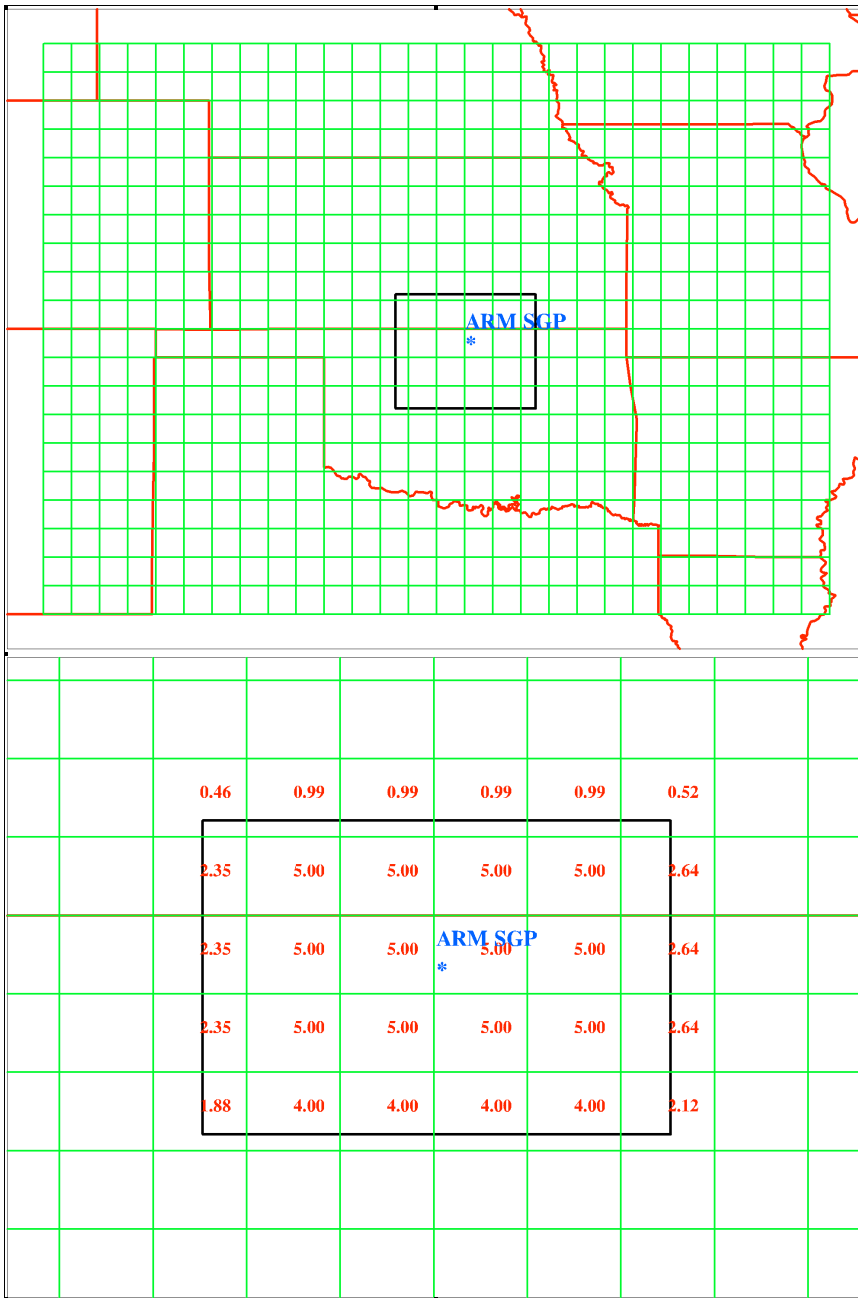
Fig. 1. Top panel: Domain for this study. The black box is the 2x2.5° SCM domain centered on the ARM SGP CF site (blue star). The green grid box represents the 0.5x0.5° grid box of GOES cloud product used in this study. Bottom panel: An enlarged 2x2.5^o grid box that includes the percentages of area from each 0.5^o box that contributed to the 2.5^o GOES average.

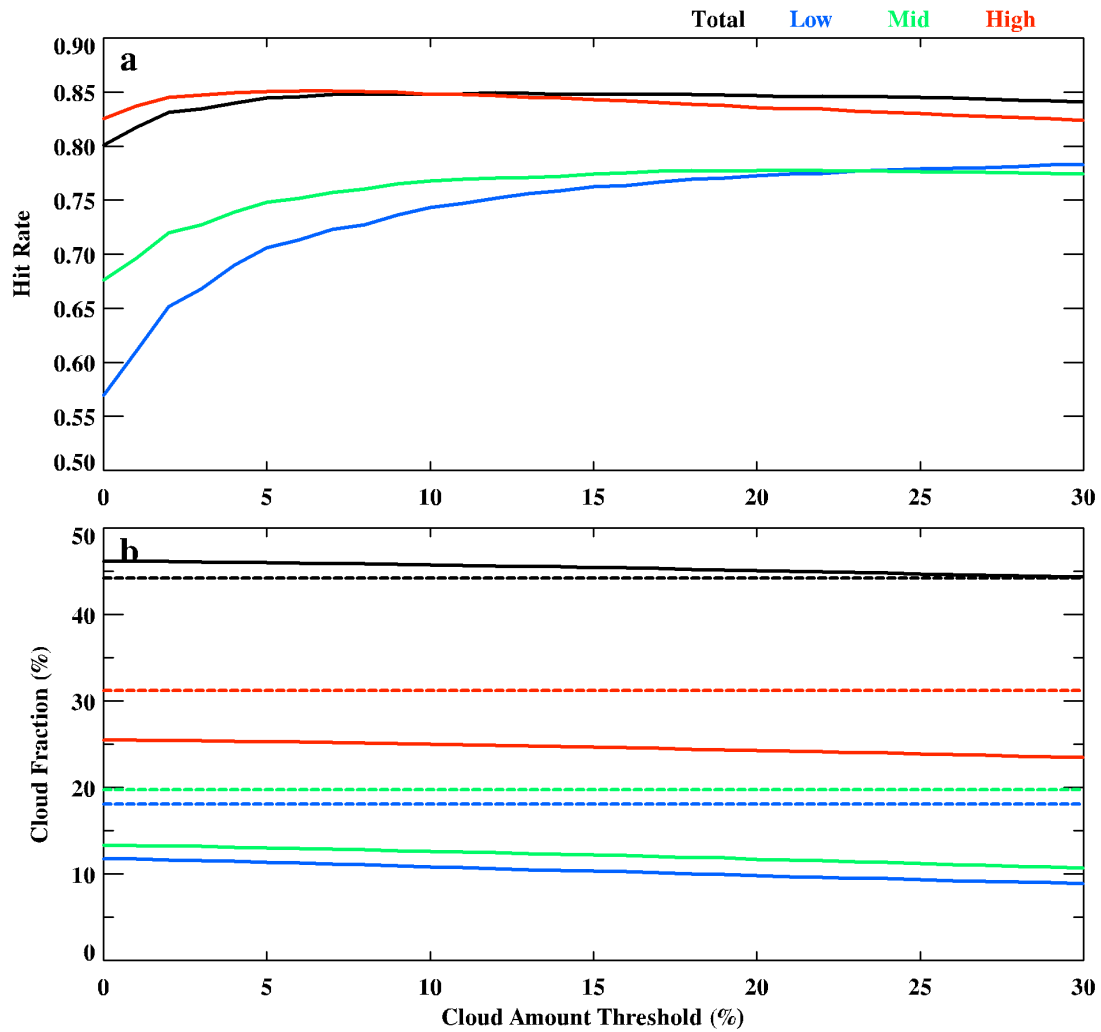Fig 2. Dependence of (a) hit rate and (b) cloud fraction on instantaneous cloud amount threshold for 0.5°×0.5° satellite observations. A threshold cloud amount is used to discriminate cloudy (≥5%) and clear scenes (<5%) in this study. Dotted lines in (b) are the radar-lidar observed cloud fractions.
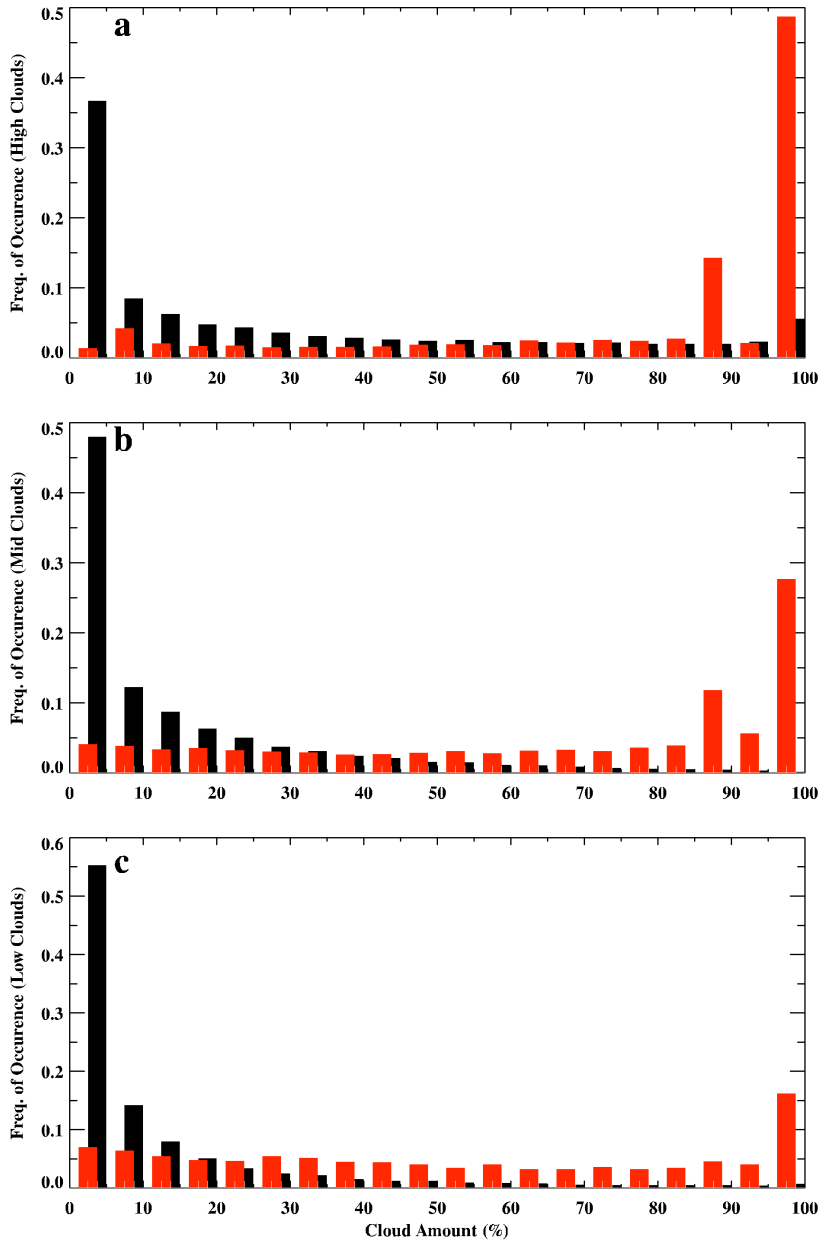
Fig. 3. Frequency distributions of cloud amount for (a) high, (b) middle, and (c) low clouds derived from GOES observations (black, before applying a threshold of 5%) and SCM simulations (red).
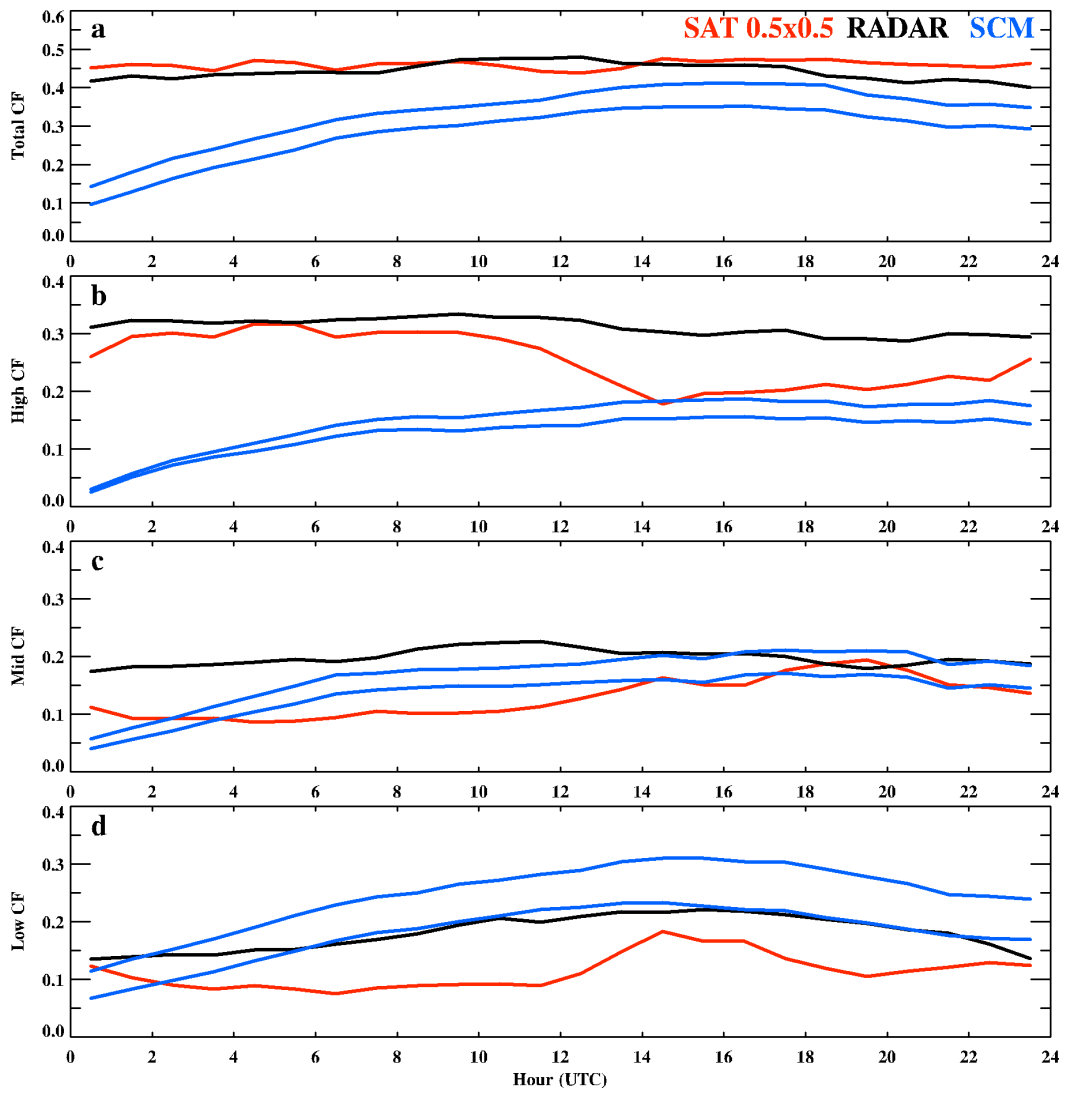
Fig. 4. Hourly means of cloud fraction for (a) total, (b) high, (c) middle, and (d) low-level clouds derived from surface radar-lidar (black), 0.5°×0.5° grid box of GOES observations (red), and SCM simulations home(blue) at ARM SGP, 1999-2001.
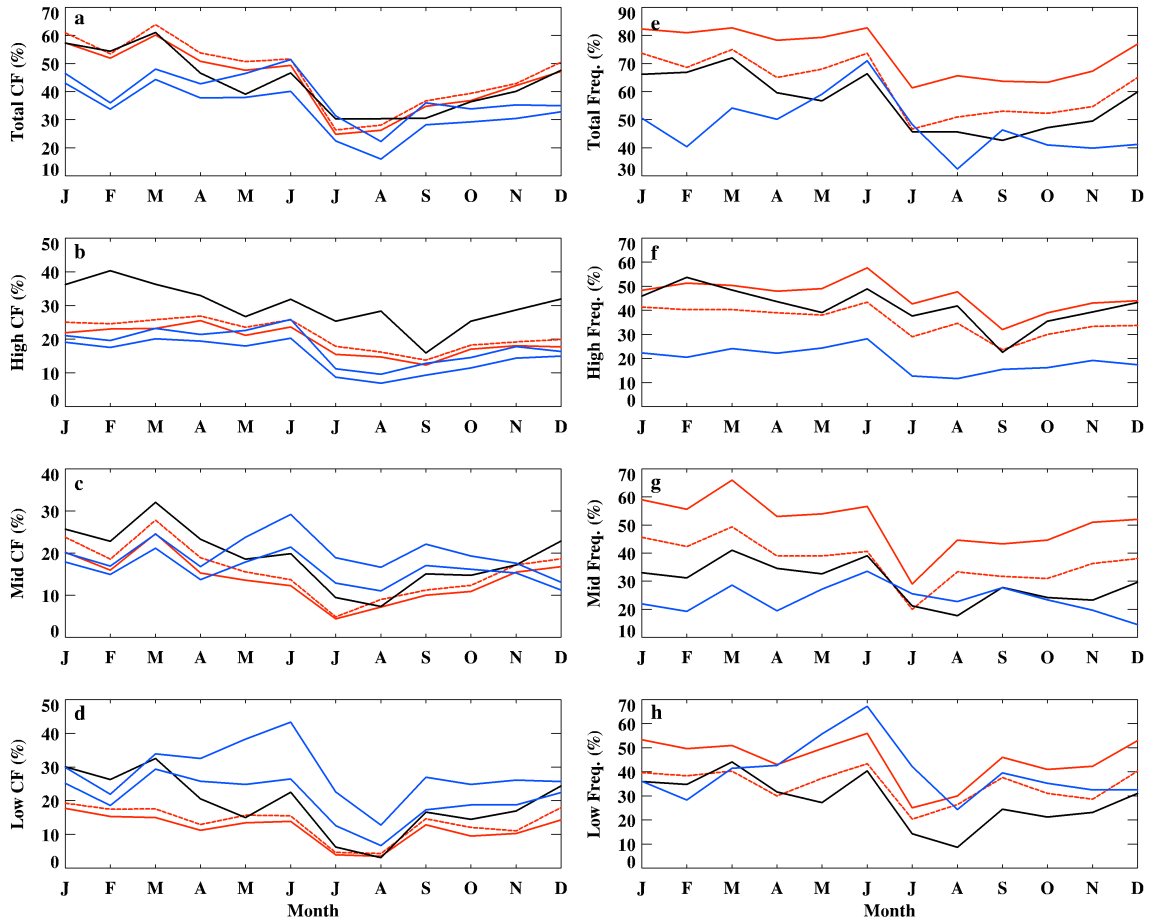
Fig. 5. Monthly mean cloud fraction (left column) and frequency of occurrence (right column) for total, high, middle and low-level clouds derived from surface radar-lidar (black), 0.5°×0.5° (solid red) and 2°×2.5° (dashed red) grid boxes of GOES observations, and 2°×2.5° grid box SCM (blue) at ARM SGP, 1999-2001.
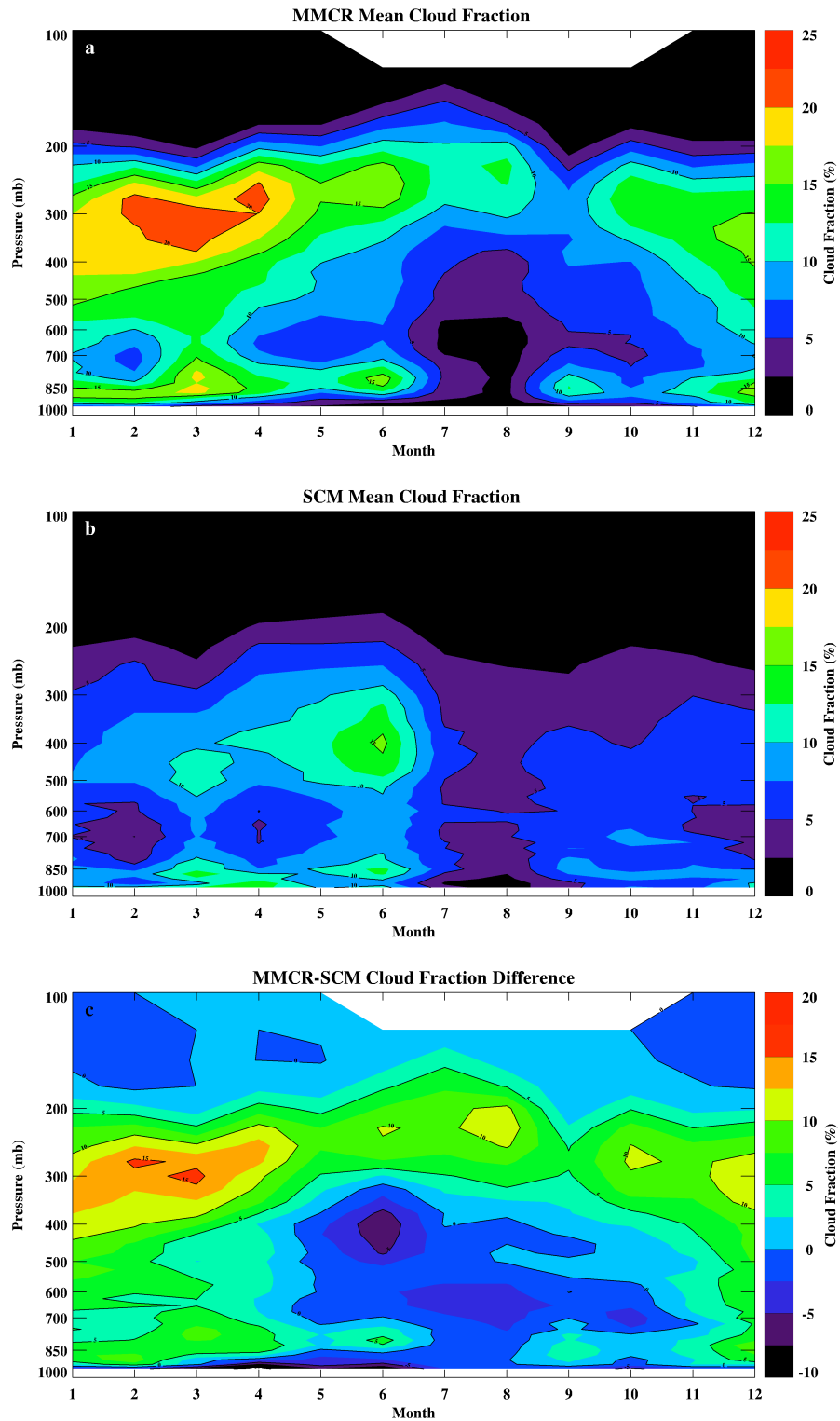
Figure 6. Monthly mean cloud fraction from 1999-2001 for (a) MMCR ground observations at ARM SGP and (b) the NASA GISS SCM model simulation. The difference between the two mean cloud fractions is given in (c).
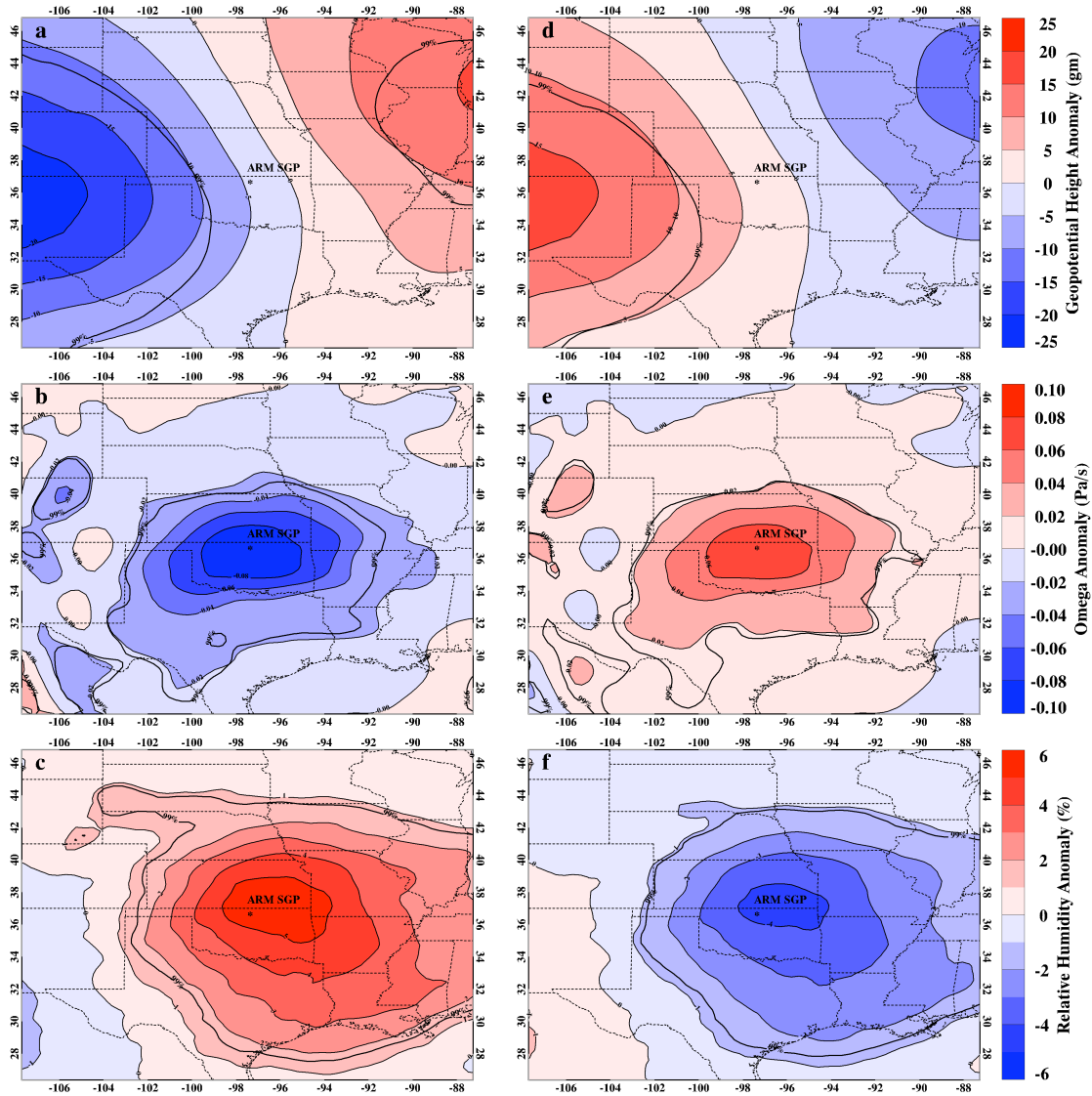
Figure 7. The 500 mb geopotential height, vertical velocity, and 300 mb relative humidity anomalies for time periods of correctly simulated high cloud cover (left column, a-c) and missed high cloud cover (right column, d-f). The thicker black lines represent the 99% significance level.
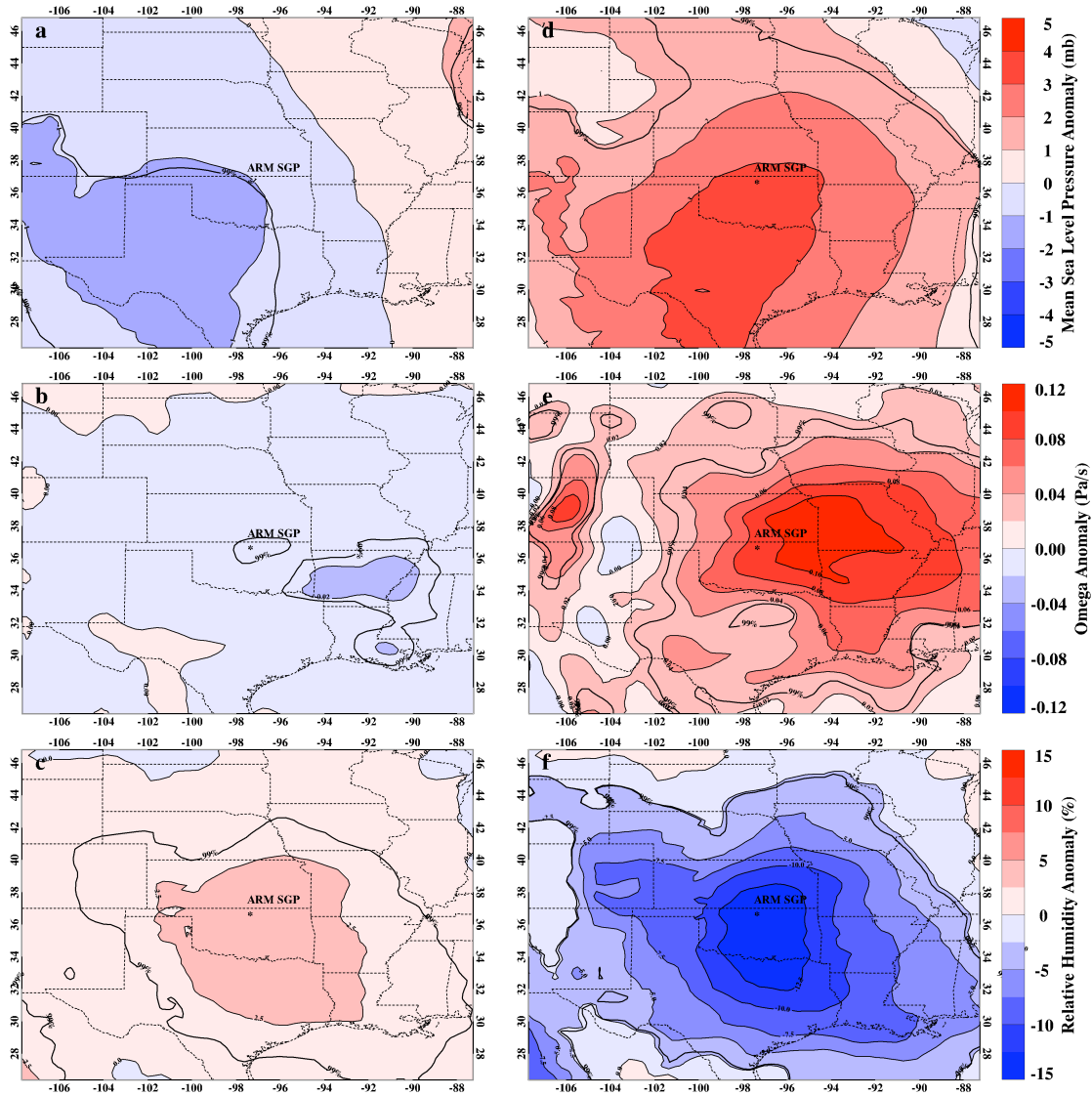
Figure 8. The Mean Sea Level Pressure (MSLP), 500 mb vertical velocity, and 925 mb relative humidity anomalies for time periods of correctly simulated low cloud cover (left column, a-c) and missed low cloud cover (right column, d-f). The thicker black lines represent the 99% significance level.
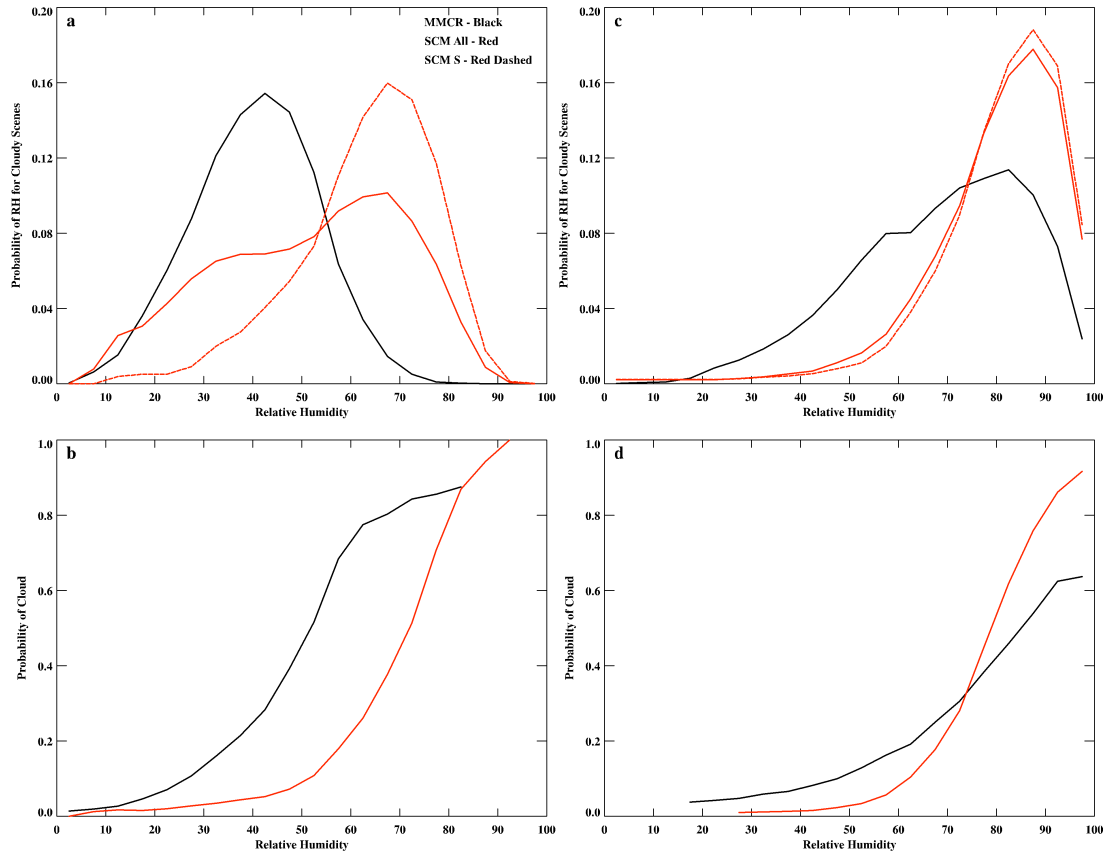
Fig. 9. Dependence of high and low cloud occurrence on relative humidity (binned to 5% increments). (a) Probability of RH observed or simulated for (total − red, stratiform − dashed red) high cloud scenes, (b) Probability of high cloud occurrence a given RH. Similar plots are shown for low clouds in c-d.
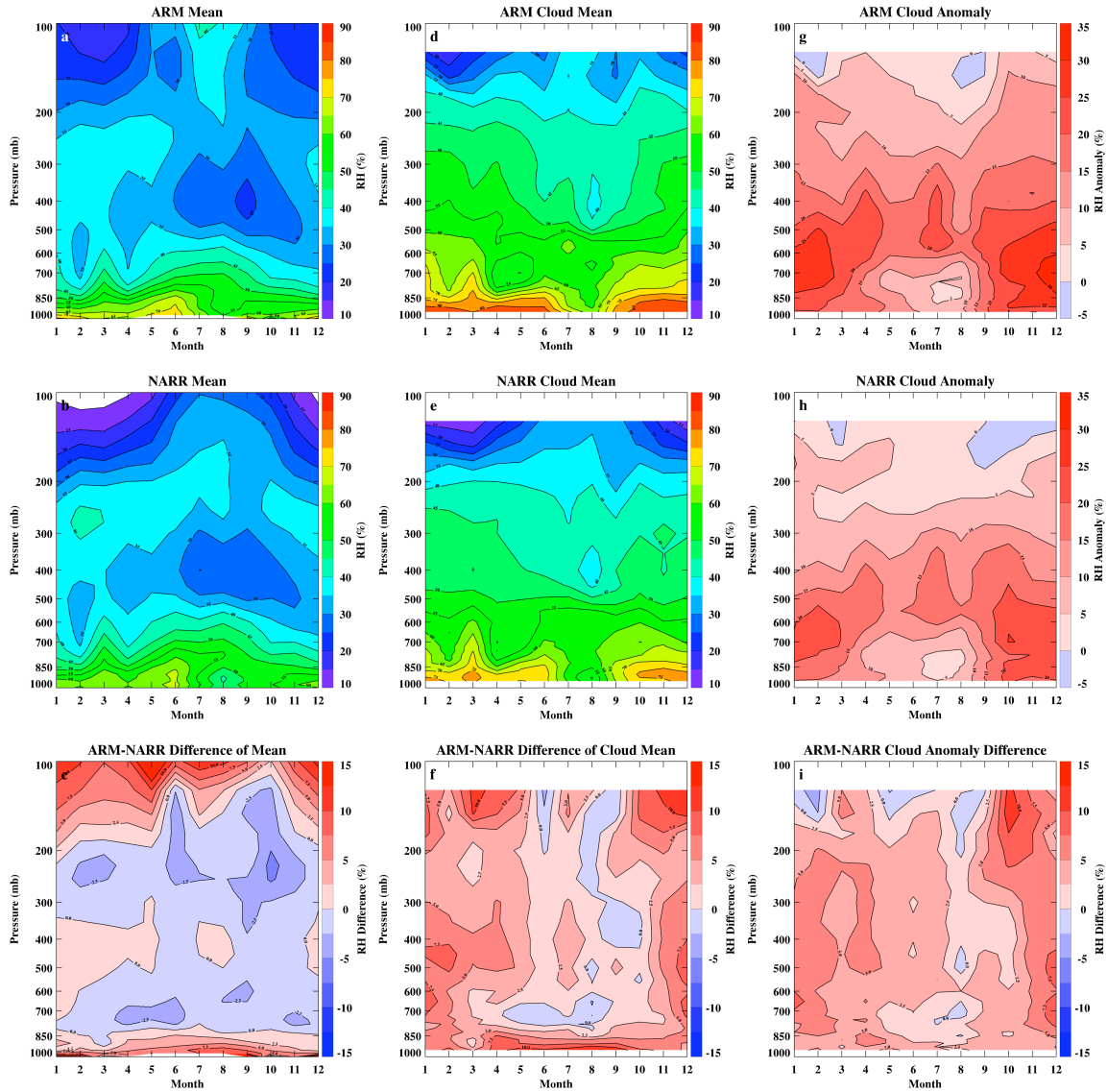
Fig 10. Monthly means of relative humidity for (a) ARM continuous forcing, (b) NARR mean for the SCM grid box, and (c) the difference between the two datasets for all-sky conditions (c). The middle column (d-f) is the same as (a-c) except for cloudy periods and the right column (e-i) is the RH difference between the cloudy and all-sky conditions. Larger values of this quantity suggest a stronger relationship between relative humidity and cloud occurrence.
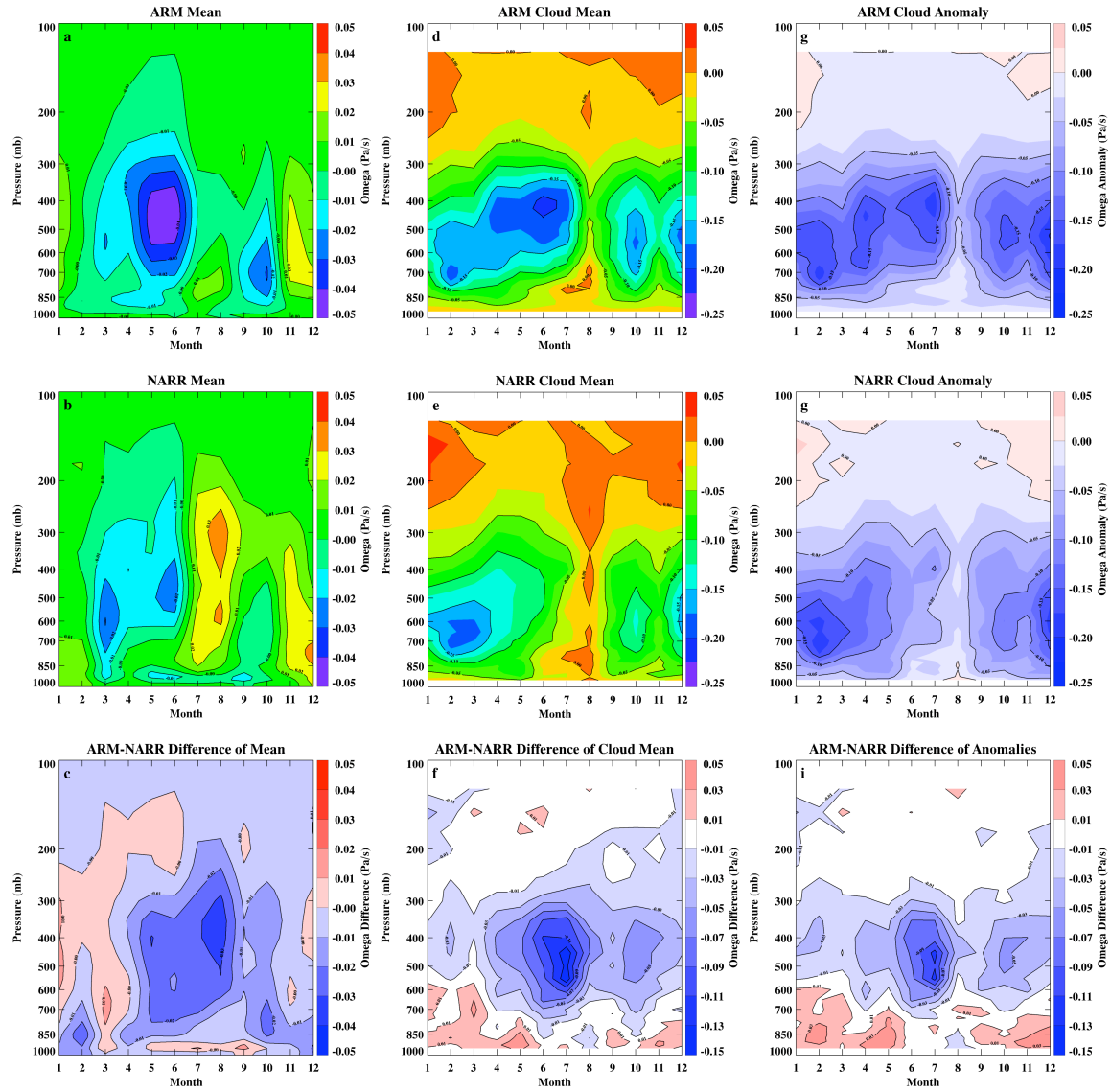
Fig. 11. Same as Fig. 10 except for vertical motion (omega).

Table 1. Resolutions of the various datasets used in this publication

Dataset	Temporal	Areal	Height
ARM SGP MMCR	5 min	< 60m (0.2° Beam)	90m
GOES VISST	~15-30 min	0.5°x0.5°	3 levels
NASA GISS SCM	1 hour	2.0°x2.5°	35 levels, ~25mb
NARR Reanalysis	3 hour	0.3°x0.3°	29 levels, ~25mb
ARM Cont. Forcing	1 hour	2.0°x2.5°	37 levels, ~25mb

Table 2. Averaged cloud fraction (CF) and frequency of occurrence (Freq) from observations and model simulations during the period of 1999-2001.

	Radar	SAT(0.5º)	SAT(2.5º)	SCM(2.5º)
	CF / Freq.	CF / Freq.	CF / Freq.	CF / Freq.
TOTAL	0.44 / 0.57	0.46 / 0.62	0.44 / 0.74	0.33-0.39 / 0.48
HIGH	0.30 / 0.42	0.21 / 0.36	0.19 / 0.46	0.15-0.18 / 0.19
MID	0.20 / 0.30	0.16 / 0.38	0.14 / 0.51	0.16-0.20 / 0.24
LOW	0.20 / 0.29	0.14 / 0.35	0.12 / 0.45	0.21-0.28 / 0.40

Table 3. Percentage of high cloud fraction occurring during stratiform conditions (omega $\geq$ 0) at the 500 mb level.

	Year	DJF	MAM	JJA	SON
RAD Percentage	0.36	0.33	0.32	0.47	0.36
SCM Percentage	0.21	0.19	0.23	0.25	0.23

Table 4. Monthly linear Pearson correlation coefficients for observed and modeled cloud fractions with (a) relative humidity and (b) vertical pressure velocity. Values are given for both the ARM continuous forcing and NARR datasets.

a. Relative Humidity

CLDFR	925mb		500mb		300mb	
	ARM	NARR	ARM	NARR	ARM	NARR
ARM TOTAL	0.65	0.73	0.7	0.72	0.84	**0.89**
ARM LOW	0.52	0.64	0.51	0.51	0.66	**0.73**
ARM MID	0.56	0.68	0.63	0.67	0.64	**0.74**
ARM HIGH	0.67	0.69	0.72	0.75	**0.85**	**0.85**
SCM TOTAL	**0.84**		0.57		0.57	
SCM LOW	**0.9**		0.42		0.51	
SCM MID	**0.61**		0.48		0.22	
SCM HIGH	**0.8**		0.62		0.64	

b. Omega

CLDFR	925mb		500mb		300mb	
	ARM	NARR	ARM	NARR	ARM	NARR
ARM TOTAL	-0.01	0.02	-0.28	-0.48	-0.37	**-0.69**
ARM LOW	-0.04	0.07	-0.18	-0.45	-0.3	**-0.65**
ARM MID	0.02	0.02	-0.21	-0.41	-0.3	**-0.59**
ARM HIGH	-0.05	-0.03	-0.35	-0.42	-0.44	**-0.62**
SCM TOTAL	-0.26		-0.6		**-0.68**	
SCM LOW	-0.25		-0.65		**-0.73**	
SCM MID	-0.27		**-0.63**		-0.63	
SCM HIGH	-0.32		-0.65		**-0.75**	

Note that the strongest correlation in each row is given in bold. Values with a magnitude greater than 0.6 are considered to have a strong correlation, while those between 0.3-0.6 are moderate, and those less than 0.3 are weak.